# Assessment of Numerical Wave Makers

# Assessment of Numerical Wave Makers

Christian Windt*†, Josh Davidson*, Pal Schmitt‡ and John V. Ringwood*
*Centre of Ocean Energy Research, Maynooth University
‡Marine Research Group, Queen's University, Belfast
†E-mail: christian.windt.2017@mumail.ie

***Abstract*—A numerical wave tank (NWT) based on Computational Fluid Dynamics (CFD) provides a useful tool for the analysis of offshore renewable energy (ORE) systems, such as wave energy converters (WECs). NWT experiments, of WEC operation, rely on accurate wave generation and absorption at the NWT boundaries. To tackle this problem, different methodologies, termed as numerical wave makers (NWMs), are available.**

**The performance of these NWMs are often sensitive to properties of the experiment being performed, such as the frequency spectrum of the input sea state, the CFD solver used and/or the internal settings of the NWM. This paper discusses the desired NWM capabilities, for effective analysis of ocean wave energy systems, and then proposes a set of test cases to assess these capabilities for a given NWM. Results are presented for a sample NWM, the OpenFOAM toolbox *OLAFOAM*, and demonstrate the sensitivity of the NWM to the desired wave conditions and the global solver settings.**

**The assessment methodologies introduced in this paper, and demonstrated for a single type of NWM, lay the groundwork for future evaluation and comparison of different NWM types, enabling appropriate NWM selection for NWT analysis of WECs.**

***Index Terms*—Numerical Wave Maker, Numerical Wave Tank, Wave Generation, Wave Absorption, OpenFOAM**

## I. Introduction

In recent years, an increased interest in high-fidelity non-linear numerical modelling of ocean wave energy systems by the means of CFD can be observed. Being able to capture all occurring hydrodynamic non-linearities, these models are applied to performance estimation [1], [2], structural analysis [3], pure hydrodynamic modelling [4] or the investigation of control strategies [5] for different types of WECs.

Like physical wave tank tests, NWTs rely on accurate wave generation and absorption for the analysis of ORE systems. Thus, it is crucial for CFD based engineering to apply reliable NWMs[1] fitted to the problem on hand. In physical wave tanks, wave generation is most significantly influenced by the applied wave generator type (flap type; piston type) and the applied control strategy [6]. The wave absorption capability reduces/removes the unwanted wave reflection from the tank boundary, and may be affected by the physical setup (beach slope; energy dissipation material) or, again, the control strategy of paddle type absorbers [7]. Limitations of wave absorption capabilities significantly hamper the representation of boundless open ocean conditions. Similarly, NWTs may also suffer from inaccuracies in the generation and absorption of waves, driving the focus of the present paper on assessment of NWM capabilities.

To tackle the NWM problem for CFD based NWTs, different methodologies have been developed. Following [8], the most prominent methods can be categorised as mass source [9], impulse source [10], static/dynamic boundary [11], and relaxation [12] methods. Their inherent differences suggests a sensitivity of numerical (WEC) studies to the selected NWM, as well as internal NWM and solver settings [13], [14]. Hence, numerical results may be biased by the applied NWM, possibly leading to incorrect power predictions or false structural load estimations. To eliminate unwanted influences from the NWM on NWT experiments, or at least quantify the (propagating) error, a rigorous assessment of the different NWMs is needed to apply the most accurate and efficient NWM for a specific problem.

As a first study, [8] delivers a qualitative evaluation of NWMs, finding significant differences in accuracy and efficiency. As a consequent sequel, this paper will discuss important NWM features that enable quality NWT experiments of WEC systems. A set of tests, and assessment criteria, are introduced to evaluate the important NWM features and to examine the sensitivity of simulation results to NWM type and applied settings. Results for a single type of NWM are presented, for illustrative purposes, and the paper aims to serve as a precursor for a subsequent rigorous assessment and comparison of multiple types of NWMs.

The paper is laid out as follows: In Section II the governing equations for the numerical solution of multi-phase problems are briefly introduced. Section III presents different NWM methodologies. Section IV introduces the important NWM characteristics for WEC experiments, and the proposed test cases to evaluate these important NWM characteristics. Section V then shows results of these test cases applied for a sample NWM. Finally conclusions (VI) and future work (VII) are presented.

## II. Computational Fluid Dynamics

The governing equations, for an unsteady and incompressible flow with constant viscosity, are the well-known Navier-Stokes equations, which describe the conservation of mass (continuity equation (1)) and momentum (Eqn. (2)).

$$\nabla \cdot \mathbf{u} = 0 \tag{1}$$

$$\frac{\partial \mathbf{u}}{\partial t} + \nabla \cdot (\mathbf{u}\,\mathbf{u}) = -\nabla p + \nabla \cdot \mathbf{T} + \mathbf{S} \tag{2}$$

[1]Due to the similarity of the numerical methods for wave generation and absorption (cf. Sec. III) the term *NWM* here embraces the capability of both wave generation and absorption

  

With fluid velocity field $\mathbf{u}$, pressure $p$, the viscous stress tensor $\mathbf{T}$ and source term $\mathbf{S}$ [15].

Additional complexity due to the multiphase problem can be captured by the *Volume of Fluid* (VOF) method proposed by [16]. The transport equation of the fluid mixture is regarded as a single fluid (Euler-Euler approach) by introducing a volume fraction $\gamma$ of the control volume (CV). In order to account for the evolution of $\gamma$ in the fluid domain, the Navier-Stokes equations are supplemented by the following transport equation

$$\frac{\partial \gamma}{\partial t} + \nabla \cdot [\mathbf{u}\gamma] + \nabla \cdot [\mathbf{u_r}\gamma \cdot (1-\gamma)] = 0 \qquad (3)$$

In Eqn. (3), the *interphase compression* term $\mathbf{u_r}\gamma \cdot (1-\gamma)$ ensures a sharp interface representation employing the additional velocity field $\mathbf{u_r}$. For further details, see [17].

The finite volume formulation is used to create the corresponding algebraic equations, from the partial differential Eqns. (1) – (3), over the computational domain represented by the mesh.

Only laminar flow conditions are consider in this paper. The assumption of laminar flow has been shown to be acceptable when modeling wave-only experiments [13] and [18], however the inclusion of turbulence when a WEC is included in the NWT simulation requires further attention.

## III. Numerical Wave Makers

To overcome the challenge of free surface water wave generation and absorption during WEC analysis, different methodologies for NWMs are available for both commercial and open-source CFD codes. Following [8], these can be categorised into five methods depicted in Fig. 1.

The **mass source** wave maker proposed by [9] displaces the free surface with a fluid inflow and outflow. A source term $s(t)$ (cf. Eqn. (4)) is defined coupling the free surface elevation (FSE) $\eta$, wave celerity $c$ and the surface area of the source $A$.

$$s(t) = \frac{2\,c\eta(t)}{A} \qquad (4)$$

The source term enables the definition of a velocity field or a volume source term for the application as boundary condition or to adapt the continuity equation, respectively. For further details see [8]. Since the source term does not alter waves travelling through the source, wave absorption can only be achieved through an additional beach, for which different methods can be found in [13], [19], [20] and are not further discussed here.

For the **impulse source** wave maker proposed by [10] a source term is added to the momentum equation, coupling the density $\rho$ and an analytical solution of the wave velocity $\mathbf{U}_{ana}$ for each cell with the geometrical scalar field of the wave maker $\mathbf{r}$ [8]. This formulation serves as an extension to the momentum equation (2), leading to

$$\frac{\partial \mathbf{u}}{\partial t} + \nabla \cdot (\mathbf{u}\,\mathbf{u}) = -\nabla p + \nabla \cdot \mathbf{T} + \mathbf{S} + \mathbf{r}\rho\mathbf{U}_{ana} \qquad (5)$$

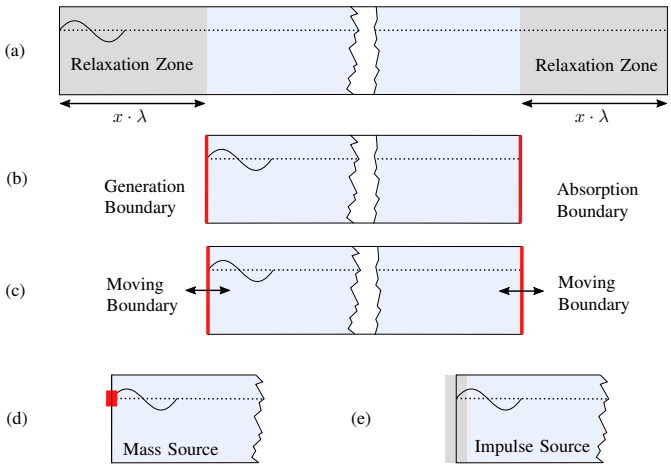


Fig. 1. Schematic representation of available NWM methodologies: (a) relaxation zone method, (b) static boundary method, (c) dynamic boundary method, (d) mass source method, (e) impulse soure method (figure adapted from [8])

Again, wave absorption can only be achieved through an additional beach.

In order to generate the desired wave field in the computational domain, [12] makes use of the **relaxation zone** method. Here, wave generation at the inlet boundary as well as wave absorption at the outlet and the inlet (internally reflected waves) can be achieved. Inside the relaxation zones, the relaxation function (6) is defined, so that the quantity $\phi$ follows Eqn. (7).

$$\alpha_R(\chi_R) = 1 - \frac{\exp(\chi_R^{3.5}) - 1}{\exp(1) - 1} \quad \text{for} \quad \chi_R \in [0;\,1] \qquad (6)$$

$$\phi = \alpha_R \phi_{\text{computed}} + (1-\alpha_R)\phi_{\text{target}} \qquad (7)$$

In Eqn. 6, the definition of $\chi_R$ ensures $\alpha_R = 1$ at the interface of the relaxation zone and open domain and $\alpha_R = 0$ at the inlet/outlet boundaries. Hence, $\phi$ is the blended solution of the numerically determine ($\phi_{\text{computed}}$) and target solution. For wave generation, the analytical solution for the target values of $\phi_{\text{target}}$ (i.e. $\mathbf{u}_{\text{target}}$ and $\gamma_{\text{target}}$) is determined from the wave theories and substituted into Eqn. (7). For wave absoprtion $\mathbf{u}_{\text{target}}$ equals zero while $\gamma_{\text{target}}$ defines the location of the still water line.

The procedure developed by e.g. [11] and [21] incorporates wave generation and absorption through the **static and dynamic boundary** method. By mimicking the wave generator/absorber using dynamic mesh motion, a dynamic boundary method represents the numerical replication of a physical test facility with all its complexities such as evanescent waves and control strategy.

Compared to the relaxation method, the static boundary method defines the velocity field and the FSE (i.e. volume fraction) as Dirichlet boundary conditions at the inlet/outlet, having the advantage of a reduced computational domain due to the absence of relaxation zones (cf. Fig. 1). At the wave generation boundary, source of the necessary data are either

the implemented wave theories or time series of physical wave maker outputs (i.e. displacement, velocity, FSE). At the absorption boundary, the determination of the necessary boundary values is based upon work by [22]. Under consideration of the shallow water theory (i.e. constant velocity profile along the water column), a correction velocity $U_c$ is applied at the boundary. For more details, the interested reader is referred to [11] and [21, chap. 5.3].

## IV. Wave Maker Capabilities

To enable NWT experiments of WEC systems, the NWM must possess two important features: (1) the capability of generating a desired wave field (either open ocean or near shore), and (2) the ability to absorb outgoing waves at the boundaries (to mimic boundless open ocean conditions). Furthermore, handling of wave structure interaction (WSI) must be possible, allowing for stable simulations of dynamic mesh motion and accurate WEC responses to simulated waves.

The aim of this section is to define test cases to evaluate the two important NWM features, (1) wave generation and (2) wave absorption. These test cases can be seen as guidelines for users to assess their NWM on hand. Note that the test cases presented herein consider a two-dimensional domain and do not claim completeness.

### A. Wave Generation

There are a variety of different wave types an ideal NWM should produce, such as: deep and shallow water waves, monochromatic and polychromatic sea states, and reproduction of arbitrary FSE time series, measured from a physical wave tanks or ocean test sites.

In vicinity of the NWM, a zone may be observed where e.g. the waves are not fully developed or evanescent waves occur (see Fig. 2). If such effects can be observed, the min. distance to the NWM has to be determined.

It has been reported by [18], [23], that NWMs, specifically when employed in the VOF framework, potentially suffer from mass defects. Monitoring a change in the mean water level or the volume fraction of the liquid phase over the duration of the simulation should be part of the assessment of a wavemaker.

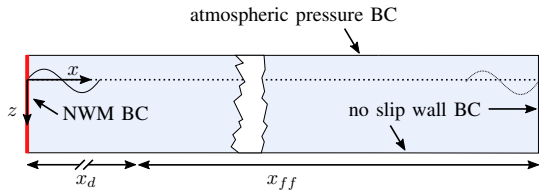


Fig. 2. Schematic of the numerical domain including boundary conditions (BCs) for the assessment wave generation capabilities: $x_d$ defines the length in which the waves are potentially biased by the wavemaker, $x_{ff}$ defines the free flow length of the domain in which the waves are travelling driven by the according hydrodynamics

To assess the wave generation performance of a given wavemaker, the following test cases are identified:

1) Deep water monochromatic sea state
2) Shallow water monochromatic sea state
3) Polychromatic sea state
4) Reproduction of time series

The following evaluation methods and metrics can be used for assessment of the wave generation capability of a given NWM for the four test cases.

*1) Deep water monochromatic sea state:* In order to get a first impression of the wave generation capabilities a simple test case can be defined by simulating of linear, 1st order monochromatic waves. Based on Airy wave theory [24] the numerical outputs, i.e. FSE and velocities, can easily be compared to analytical values. Specifically, the root-mean-square error (RMSE) between numerical and theoretical FSE data and the max. relative error between numerical and theoretical horizontal fluid velocity will be taken as quantification for the wave generation capability.

The total volume fraction of water in the NWT should be measured to ensure mass conservation, in this test and all the others.

*2) Shallow water monochromatic sea state:* Characteristics of shallow water waves should also be represented correctly. However the analytical solutions are much more complex [25]. As for deep water, the RMSE between numerical and theoretical FSE serves as a quantification for the wave generation quality.

*3) Polychromatic sea state:* The simulation of monochromatic waves is of interest for simple test cases or to find the dependency of system characteristics to distinct wave lengths and wave heights. However, to mimic real sea conditions, the representation of polychromatic sea states is of interest, providing more realistic WEC power and load estimations from the NWT simulation. Hence the capability of a NWM to reproduce spectral sea states parametrised by significant wave height $H_s$ and peak period $T_p$, is of importance.

The accuracy of reproducing polychromatic waves can not simply be assessed by comparing analytical to numerical FSE data. In fact, the achieved measured output spectrum has to be compared to the theoretical input spectrum using the spectral distribution from Fast Fourier Transforms (FFTs) of the according signals. Qualitative comparison is achieved by simply comparing the shape of the input/output signal spectrum. Quantification can again be achieved by comparing the RMSE of the spectral distribution between desired and measure spectral sea states.

*4) Reproduction of time series:* The capability of reproducing exact FSE time series, enables high-fidelity validation against experiments performed in real wave tanks, reproduction of extreme wave conditions for WEC survivability, and replication of a pre-measured input time series from a possible WEC deployment location. For this paper, the assessment is binary, only checking whether a NWM has the ability to reproduce any time series or not, without further specifying or quantifying possible errors.

### B. Wave Absorption

The capability of absorbing waves travelling from the WEC towards the far field boundaries (FFB) is crucial for an efficient NWT, [26]–[28]. Wave reflection, quantified by the reflection coefficient $R$ as the ratio of incident and reflected waves, should ideally be eliminated ($R = 0$), or at least mitigated ($R << 1$), by the NWM. By eliminating reflected waves, the NWM allows the NWT to replicate open ocean conditions, which can otherwise only be achieved by extending the computational domain towards infinity, at immense computational cost. Whilst eliminating the reflected waves, the NWMs must also ensure that the generation of input waves into the NWT is not corrupted by the absorption of the outgoing waves.

To assess the wave generation performance of a given wavemaker, the following test cases are identified:

1) Absorption at the wave generator

Absorption at the FFB:

2) Deep water monochromatic sea state
3) Shallow water monochromatic sea state
4) Polychromatic sea state
5) Waves radiated from a WEC

The following evaluation methods and metrics can be used for assessment of the wave absorption capability of a given NWM for the five test cases.

*1) Absorption at wave generator:* The presence of bodies, fixed or floating, in the NWT, causes wave reflection/radiation, travelling away from the bodies towards the wave generator boundary. To generate the desired, steady wave field, the NWM control has to account for these outgoing reflected/radiated waves. The quality of generated waves, in NWTs incorporating bodies (such as WECs), is affected by the capability of the generation boundary to handle outgoing waves. The test case here 1), considers the most extreme case of a reflective body, a full reflective wall.

Generating a monochromatic wave into a NWT domain, with a fully reflective wall oppposite the wave generator, leads to the build-up of a standing wave. Due to the governing physics, the amplitude of the standing wave $A_s$ is expected to be equal or smaller to twice the incident wave amplitude $A_i$. Moreover, distinct constant location and velocity profiles of nodes and anti-nodes along the NWT, should be observed.

For the evaluation of the quality of wave absorption at the wave generation boundary, the characteristics of the standing wave can be investigated. Quantification is delivered by the ratio $A_s/A_i$. Qualitative assessment can be achieved by inspecting the (anti-)node location and velocity profiles.

*2) Absorption at FFB: Deep water monochromatic sea state:* A simple test case for assessing the NWM absorption capabilities, can be found in simulating linear, 1st order monochromatic sea states at the generating boundary, like in Sec. IV-A1, and then calculating the reflection coefficient at the FFB. The reflection coefficient is a good metric for the absorption quality of the NWM, and can be calculated by measuring the FSE, using a three point method proposed by [29], from which incident and reflected waves can be separated and the reflection coefficient determined.

*3) Absorption at FFB: Shallow water monochromatic sea state:* Since numerical wave absorption may be dependent on the underlying theory upon which it is implemented, the capability of absorbing shallow water waves should be investigated. The same setup as in IV-B2 is applied and reflection coefficients are calculated for monochromatic cnoidal shallow water waves.

*4) Absorption at FFB: Polychromatic sea state:* Polychromatic sea states, are more representative of real sea conditions, than monochromatic waves. Efficient wave absorption must be available over a given frequency range (and directions for 3D tanks). The reflection coefficient serves as a metric for the absorption quality of the NMW.

*5) Absorption at FFB: Waves radiated from a WEC:* So far, *wave-only* cases have been considered in the assessment of NWM capabilities. In order to analyse WECs, WSI must be accounted for in the NWT. WEC motion adds complexity to the CFD simulation, whereby distortion, motion or topological changes of the mesh might affect the NWM performance.

A free decay experiment can be applied to isolate and assess the absorption abilities of the NWM. In particular, the free decay experiment focuses on the absorption of waves, whose properties (frequency and amplitude etc), naturally lie in the hydrodynamic region that will likely be radiated by the WEC. Additionally, the free decay experiment provides a gentle way to test the body motion solver coupling with the combined CFD - NWM solver. The NWMs may have a degree of sensitivity to the quality of the mesh, which can be tested gently by selecting the initial amplitude of the free decay experiment.

In the free decay experiment, the body is given a known initial amount of energy, via its nonequilibirum intial value for displacement and/or velocity. The fluid is set initially at rest and no external energy should be added to the NWT. Therefore, tracking the energy throughout the free decay simulation is a useful indicator to assess the NWM absorption abilities. The energy should be radiated away from the body and be absorbed by the NWM, with no energy being reflected back towards the body. Position, velocity or acceleration data can be measured showing an exponentially decaying transient signal.

## V. Test Results for Sample Wave Maker

In this section, the test cases, and assessment guidelines, defined in Section IV, are applied to a sample NWM and results presented.

### A. Sample wave maker

Numerous commercial, open source and academic software tools are available to perform CFD analysis of WSI. One of the most prominent open source representatives is the OpenFOAM toolbox [30]. This C++ based package includes several numerical solvers for a wide range of physical problems. Supported by a large user community, avoiding license purchase and

enabling source code tailoring, OpenFOAM is widely applied in industry and academia [1], [5], [31]. The implementation of an OpenFOAM NWT for wave energy experiments is detailed in [32].

The test cases presented in this section are simulated in an OpenFOAM NWT, using the *OLAFOAM* toolbox as a sample NWM. Developed by [11], [21], OLAFOAM is derived from the IHFOAM NWM [33] and based upon the OpenFOAM multiphase solver interFOAM. The NWM incorporates both the static or dynamic boundary methods to achieve wave generation and absorption. The static boundary method is selected as the sample NWM for the results presented herein (the dynamic method requires $20-40\%$ increased computational effort compared to the static method [21]). For detailed information on the governing eqautions and solution methods, the interested reader is referred to the above given references.

*1) Mesh convergence:* Due to the nature of the solution process employed by CFD, convergence studies on the spatial and temporal discretisation have to be performed before running simulations for the NWM test cases. For the sake of brevity we only present parts of the results here. Figs. 3-a) and b) show the deviation between FSE gained from subsequently refined meshes to the finest mesh in both vertical (Fig. 3-a)) and horizontal (Fig. 3-b)) direction. Results are normalised by the wave amplitude $A$. Convergence is achieved for a spatial discretisation of $\Delta x = {}^{\lambda}/_{160}$ and $\Delta z = {}^{H}/_{32}$, henceforth referred to as base mesh. To prevent large cell counts, mesh refinement towards the free surface is applied. A snapshot of the spatial discretisation is shown in Fig. 4. Furthermore, convergence of the temporal discretisation is achieved employing adjustable time-stepping limited by a maximum allowed Courant number of $Co_{max} = 0.5$. Most efficient simulations are performed using parallel high performance computing (HPC) with approximately 30000 cells per core. All cases are parallelised to ensure most efficient computation.

As mentioned in Section III, the static boundary method sets wave parameters (i.e. velocities, FSE) as Dirichlet boundary condition directly at the domain boundary. The nature of the VOF method therefore suggests a dependency of the quality of generated and absorbed waves on the mesh discretisation at the boundary. Although convergence studies on the discretisation around the free surface interface have been performed, increased accuracy might be achieved by refining/coarsening the mesh discretisation in the vicinity of the NWM. The influence of this mesh discretisation, upon the test case results, for the sample NWM is investigated in the following sections.

### B. Wave Generation

*1) Deep water monochromatic sea state:* The test case example here, considers a deep water monochromatic wave with height $H = 0.02\text{m}$, period $T = 1.6\text{s}$ and length $\lambda = 4\text{m}$ (adapted from [34]). To enable assessment of wave generation effect only, contaminating effects of reflected waves

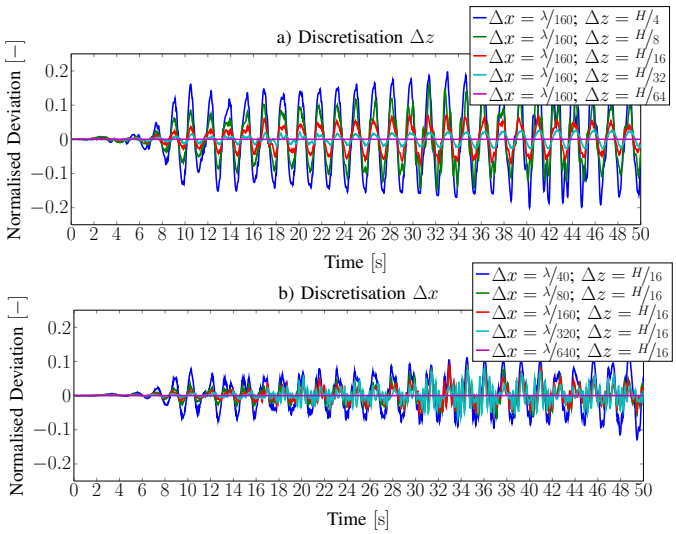


Fig. 3. Mesh convergence study: Deviation of FSE (normalised by wave amplitude), for different mesh resolutions, compared to the finest mesh case

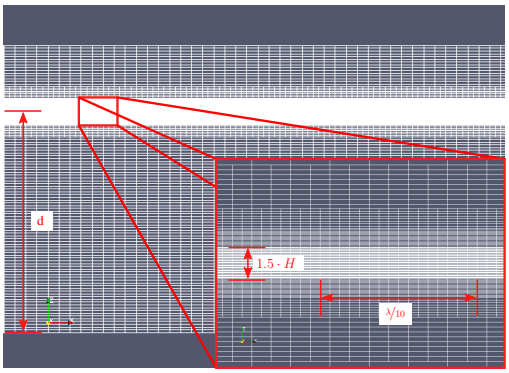


Fig. 4. Snapshot of the computational mesh: Discretisation around the free surface with $\Delta x = {}^{\lambda}/_{160}$ and $\Delta z = {}^{H}/_{32}$

are avoided by extending the tank length $x_d + x_{ff}$ to $100\text{m}$ (cf. Fig. 2) and limiting the simulated time to $t = 40\text{s}$.

The FSE is measured a numerous locations in the NWT during this experiment. The RMSE, between the measured FSE and the analytical values, provides a metric for the assessment of the NWM performance. FSE data can be readily obtained from the NWT, by tracking the iso-surface of the fluid volume fraction at $\gamma = 0.5$.

The RMSE value, between the analtyically predicted FSE values and the FSE measured in the NWT, is herein obtained by averaging the measured FSE amplitude in the NWT over 20 repeating halfwave periods. To neglect transient effects, averaging begins after $25\text{s}$ of simulation time. From the time averaged data, mean FSE values, along with upper and lower bound standard deviations ($\sigma$), are calculated. Results at four different locations in the NWT (cf. Fig. 5) are plotted and compared against the analytical solution in Fig. 6.

Using this measure, the influence of the spatial discretisation in the vicinity of the generation boundary is analysed. Generally, an improvement of the wave quality, represented by low

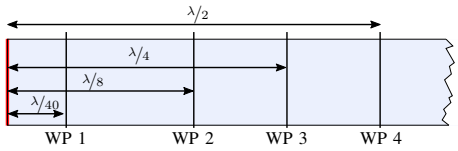


Fig. 5. WP location for FSE data extraction in NWT: Wave generation at left boundary

RMSE values, is expected for the case of finer discretisation in vicinity of the generation boundary. From the analysis of the RMSE, good wave generation quality employing a mesh with $\Delta x = \lambda/160$ and $\Delta z = H/32$ at the free surface (base case) can be observed. An unexpected result is that finer mesh discretisation is found to increase the RMSE. Investigation of the influence of e.g. transition regions between different discretisations should hence be part of future work. For the base case, lowest RMSE values ($< 0.5 \cdot 10^{-3}$) are found up to $x_5 = 3/4\lambda$. After that, due to numerical dissipation, higher deviations are observed.

Velocity profiles are evaluated along a vertical profile of velocity probes in the NWT. To simplify the comparison against analytical data, only the time instances at wave crests or troughs are measured along the vertical profile of velocity probes. Fig. 7 shows the horizontal water velocity[2] gained from the analytical solution and measured in the NWT. Again, satisfying agreement between the analytical and numerical solutions is found. The maximum relative error is found to be $< 6\%$ at the wave trough at a water depth of $1.8\text{m}$.

Lastly, inspecting the deviation of the instantaneous total volume fraction of the liquid phase to the initial target value, only negligible deviations, on the order of $10^{-5}$, are observed, implying mass conservation throughout the simulation. Results for the test cases are summarised in Table I.

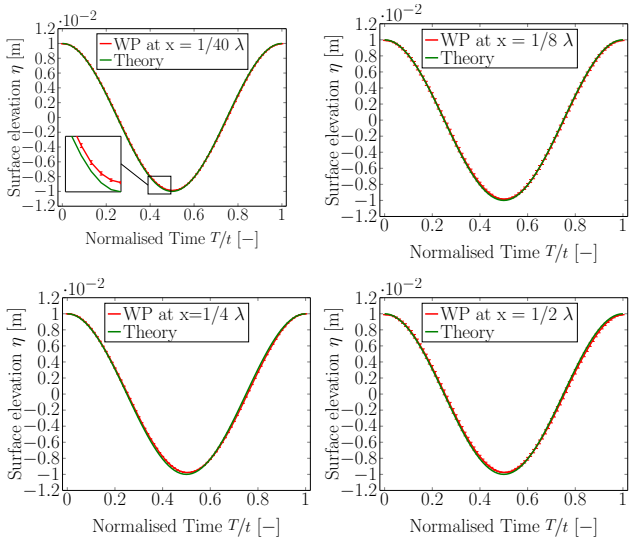


Fig. 6. Time averaged FSE data (red) compared to analytical solution form Airy wave theory (green) at different WPs

[2]Due to their small magnitude, vertical velocities are omitted in Fig. 7

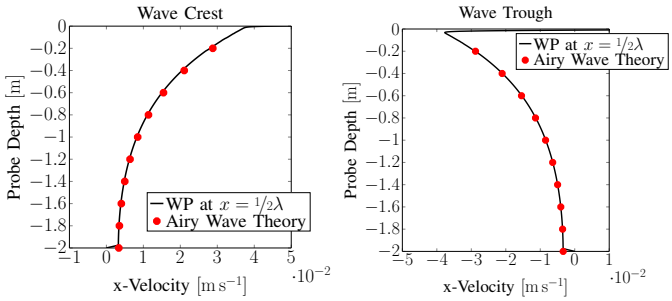


Fig. 7. Velocity profiles for increasing depth beneath wave troughs and crests, calculated from Airy wave theory and measured $1/2\lambda$ from the wave maker

*2) Shallow water monochromatic sea state:* The test case example here considers a monochromatic shallow water wave, with height $H = 0.1\text{m}$, period $T = 3\text{s}$ and length $\lambda = 5.77\text{m}$. The water depth $d$ is set to $0.4\text{m}$. The NWT length is set to $x_d + x_{ff} = 100\text{m}$ and simulated time is limited to $t = 40\text{s}$.

Like the evaluation of deep water wave generation, the quality of the shallow water wave generation, and its dependency on the mesh in the vicinity of the generation boundary, will be determined by the RMSE between measured and theoretical values. Following the procedure in Section V-B1, the FSE at different tank locations is averaged over 10 wave periods and mean, upper and lower bound RMSE values are calculated.

To determine the mesh dependency, simulations with identical BCs are ran with varying spatial discretisation in vicinity of the generation boundary (cf. Fig. 8), leading to five different cases:

- *B*: with the base mesh over the entire domain
- *TT*: with half the cell size over a length of $1/4\lambda$
- *TTS*: with half the cell size over a length of $1/10\lambda$
- *FT*: with a quarter the cell size over a length of $1/4\lambda$
- *FTS*: with a quarter of the cell size over a length of $1/10\lambda$.

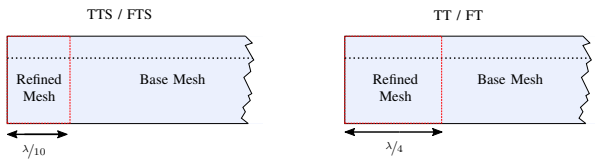


Fig. 8. Schematic of the varying discretisation in the vicinity of the wave generation boundary

Fig. 9 shows the results for eight different WP locations. The results show similar *wave quality* up to $0.35\lambda\,(= 2\text{m})$, where a RMSE of around $3 \cdot 10^{-3}$ can be observed. Subsequent, *wave quality* decreases for the cases *B*, *TT*, *TTS*, whereas the two cases *FT*, *FTS* show similar mean RMSE values of around $3 \cdot 10^{-3}$. Taking the run time for the different cases into consideration, it can readily be stated, that case *FTS* with a reduced run time of around $40\%$ compared to *FT*, is the most efficient setup amongst the tested cases.

However, it must be noted, that the generation of shallow water Cnoidal waves with the tested characteristics lacks accuracy. The achieved RMSEs show values about three times

higher compared to the case in V-B1. Inspecting the results plotted in Fig. 10, shows large deviations of trough values as well as shape distortion downstream in the NWT.

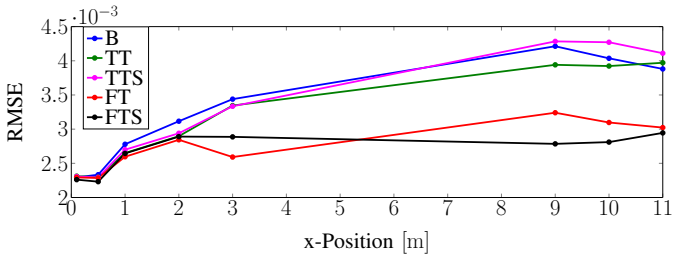


Fig. 9. Mean RMSE for five different spatial discretisations (*B*, *TT*, *TTS*, *FT*, *FTS*) evaluated at eight different WP locations

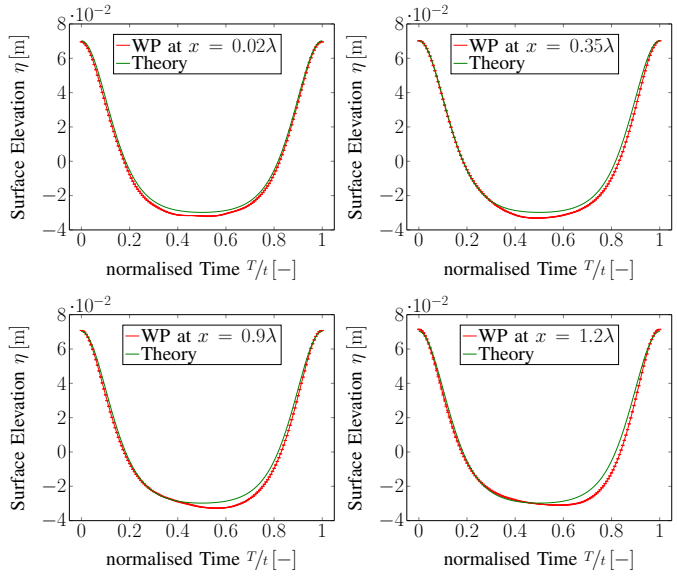


Fig. 10. Time averaged FSE data (red) compared to analytical solution form Cnoidal wave theory (green) at different WPs

*3) Polychromatic sea state:* The test case example here, considers a JONSWAP spectrum, with $H_s = 0.094\text{m}$, $T_p = 1.65\text{s}$, $\gamma = 1$ in $d = 2.2\text{m}$ water depth. The NWT length, $x_d + x_{ff}$, is extended to $200\text{m}$ and $t$ limited to $100\text{s}$.

The evaluation of the polychromatic sea states, is performed by comparison of the power spectral density (PSD) of the measured FSE values, against the analytical PSD (based upon [35]) of the input JONSWAP spectrum.

Fig. 11 shows the considered input spectrum (dashed red line) and the output spectra, gained from FFT of the FSE data measured $0.5\text{m}$ (blue line) and $8\text{m}$ (black line) from the NWM.

The input spectrum shows a peak at a frequency of $1/T_p = 0.6061\text{s}^{-1}$, matching the desired input of $T_p = 1.65\text{s}$. Inspection of the measured spectra reveals an overall good fit to the input with a normalised RMSE (NRMSE) of 0.16. However the peak frequency is shifted by $\approx 6\%$ at both WP locations. In fact, the output spectra show a drop at the expected peak frequency and further investigation of this observation is required.

Comparing the two measured spectra, negligible differences can be observed up to a frequency of $0.65\text{s}^{-1}$. However, for higher frequencies, differences become more significant. Better agreement between the theoretical input and the measured PSD can be observed at the WP $8\text{m}$ downstream. The influence of proximity to the NWM on the measured wave spectrum, should be well understood when designing the NWT length (see Fig. 2) to allow optimal placing of the WEC within the NWT for efficient, accurate simulations.

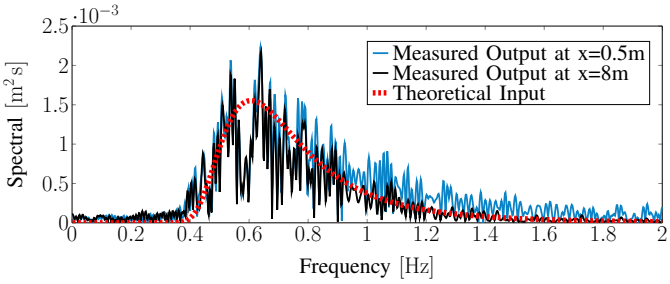


Fig. 11. Theoretical PSD (dashed red line) and NWT PSD measured $0.5\text{m}$ (blue line) and $8\text{m}$ (black line) downstream from the NWM

*4) Reproduction of time series:* The sample NWM provides the possibility to reproduce given time series (FSE and velocity) using the static boundary method in the *OLAFOAM* toolbox. Fig. 12 shows a given time series of the piston displacement $x_P$, that is to be replicated by the NWM, and the measured FSE $\eta$ at two WP locations. Inspection of the input and output (i/o) time series suggests, that the period of i/o matches well throughout the simulation. However, differences in the wave shape can be observed when comparing FSE data extracted at $x = 0.5\text{m}$ and $x = 1\text{m}$. Further investigation of this effect should be part of future work.

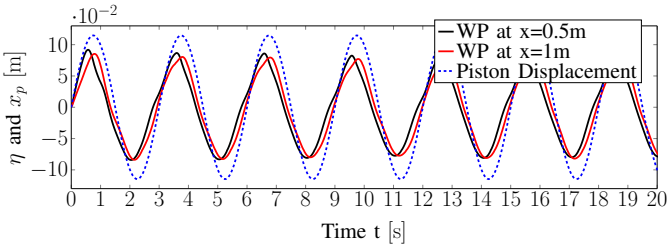


Fig. 12. Time series of piston displacement $x_P$ (input) and surface elevation $\eta$ (output) at $0.5\text{m}$ and $1\text{m}$ downstream

## C. Wave Absorption

*1) Absorption at wave generator:* Input wave conditions, and mesh convergence, for this test case are adopted from test case IV-A1. However, in this test, the NWT length is varied between experiments to investigate possible influence on the expected characteristics of the generated standing wave. Four different $x_{ff}$ (with $x_d$=0) were investigated, $x_{ff} = 0.5\lambda$, $1\lambda$,

TABLE I
RESULTS FOR BENCHMARK CASES TO EVALUATE WAVE GENERATION

| Case | Quantification | *OLAFOAM* |
|---|---|---|
| 1) | Max. Distance to NWM | $\approx 1\lambda$ |
| | Max. RMSE ($\eta$) | $2.2 \cdot 10^{-4}$ |
| | Max. Relative Error ($u$) | $< 6\%$ |
| | Fluid Mass Conservation (yes/no) | yes |
| 2) | Max. Distance to NWM | $\approx 1.2\lambda$ |
| | Max. RMSE ($\eta$) | $3.5 \cdot 10^{-3}$ |
| 3) | NRMSE Measured Output to Theory | 0.16 |
| | Peak Frequency Shift | $\approx 6\%$ |
| 4) | Time series reproduction | yes |

$3.25\lambda$, $4.4\lambda$. For the sake of brevity, only the case $x_{ff} = 3.25\lambda$ is depicted in Fig. 13.

Neglecting transient effects, consistent node and anti-node locations are expected, and indeed can be observed in Fig. 13. Furthermore, the NWT length was found to influence the location of the (anti-)nodes. Inspecting the maximum amplitude of the (standing) wave $A_s$ for varying NWT length, it becomes apparent that for longer tanks ($x_{ff} > 1\lambda$), $A_s$ exceeds the theoretical limit of $A_s = 2 \cdot A_i$. For example, values for $A_s/A_i$ of 2.7 can be observed at wave crests in Fig 13. Investigation of the transient behaviour by following a single wave crest travelling through the tank reveals that the unexpected $A_s/A_i$ ratios arises from reflection of waves off the inlet boundary wall. This suggests insufficient wave absorption at the wave generator by the NWM.

Plots of the velocity profile, measured at distinct (anti-)node locations, are omitted due to space restrictions. However, it can be stated, that these profiles are dominated by horizontal fluid velocity at the anti-nodes and vertical fluid velocity at the nodes, as expected by theory. Results are summarised in Tab. III.

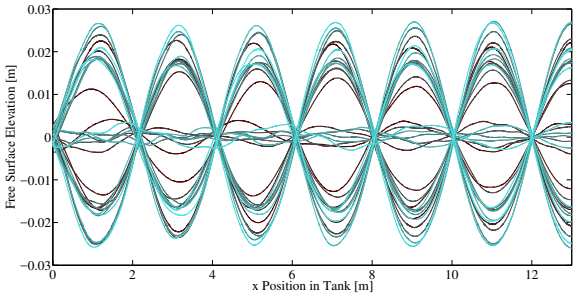


Fig. 13. FSE over tank length for $x_{ff} = 3.25\lambda$ at distinct time instances: The brighter the plot lines, the further the simulation is advanced in time

*2) Absorption at FFB: Deep water monochromatic sea state:* Wave conditions are adopted from test case IV-A1. The NWT length is set to $x_{ff} + x_d = 8\lambda$, $t$ is limited to 50s.

An influence from the mesh discretisation in the vicinity of the FFB, is expected on the NWM absorption ability. Hence, parameter studies on the mesh discretisation were performed (cf. Fig. 14 and Tab. II). Fig. 15 shows the (a) cell count , (b) run time and (c) reflection coefficient for the 8 different cases listed in Tab. II.

In Fig. 15-c) generally, poor absorption quality can be observed with a reflection coefficient $0.262 < R < 0.292$. Moreover no positive influence on the wave absorption can be observed when in- or decreasing the spatial discretisation in the vicinity of the far field boundary. It can be assumed that the poor performance stems from the applied shallow water wave theory for the calculation of the correction velocity [11], [21]. This hypothesis will be backed up by results in V-C3. Mass conservation throughout the simulation can be observed for all 8 different cases. Results are summarised in Tab. III.

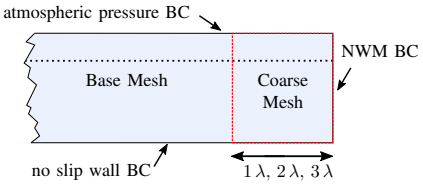


Fig. 14. Schematic of the varying discretisation in the vicinity of the wave absorption boundary

TABLE II
MESH CHARACTERISTICS FOR WAVE ABSORPTION PARAMETER STUDY WITH LINEAR, 1ST ORDER AND CNOIDAL MONOCHROMATIC WAVES

| Case # Linear | Case # Cnoidal | Mesh Characteristic |
|---|---|---|
| #1 | #1 | $1/2$ cell size of base case over $1\lambda$ upstream |
| #2 | #2 | 2x cell size of base case over $1\lambda$ upstream |
| #3 | #3 | 2x cell size of base case over $2\lambda$ upstream |
| #4 | | 2x cell size of base case over $3\lambda$ upstream |
| #5 | #4 | 4x cell size of base case over $1\lambda$ upstream |
| #6 | #5 | 4x cell size of base case over $2\lambda$ upstream |
| #7 | | 4x cell size of base case over $4\lambda$ upstream |
| #8 | #6 | Base case $\Delta x = \lambda/160$ and $\Delta z = H/32$ |

*3) Absorption at FFB: Shallow water monochromatic sea state:* Wave conditions are adopted from test case V-B2. A similar parameter study, as in test case V-C2, is performed to investigate the influence of spatial mesh discretisation on NWM absorption, for the case here of shallow water waves (cf. Fig. 14 and Tab. II). Fig. 16 shows the (a) cell count, (b) run time and (c) reflection coefficient for the first 6 cases listed in Tab. II.

Satisfactory absorption quality can generally be observed in Fig. 16-c), quantified by a reflection coefficient of $R < 4 \cdot 10^{-2}$. For this shallow water wave case, a coarsened mesh is observed to have a positive influence on the NWM absorption performance, leading to a minimum reflection coefficient of $R \approx 4 \cdot 10^{-3}$ for case #5. The results of the shallow water wave versus the deep water waves, underlines the hypothesis in V-C2, that the wave absorption performance of a given NWM, is highly influenced by the type of waves considered. Results are summarised in Tab. III.

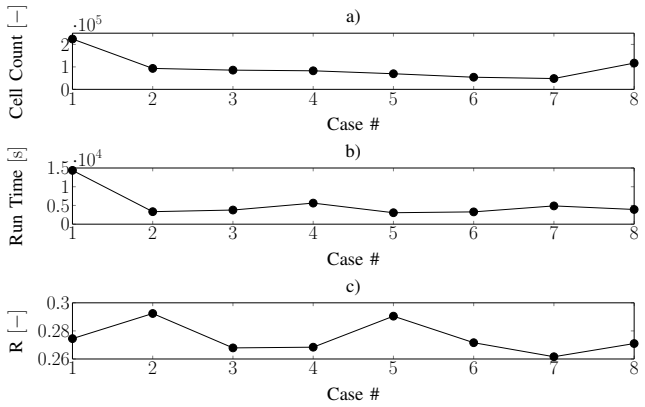


Fig. 15. Cell count (a)), run time (b)) and reflection coefficients (c)) from parameter study on the discretisation in vicinity of the FFB considering linear, 1st order monochromatic deep water waves

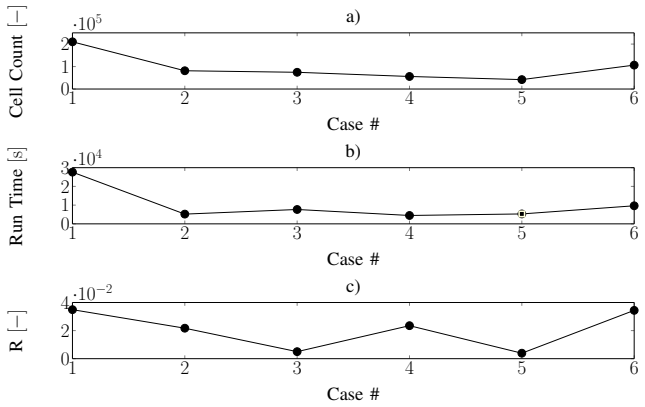


Fig. 16. Cell count (a)), run time (b)) and reflection coefficients (c)) from parameter study on the discretisation in vicinity of the FFB considering cnoidal monochromatic shallow water waves

*4) Absorption at FFB: Polychromatic sea state:* Wave conditions are adopted from test case V-B3. $x_{ff}$ is set to 50m and the simulated time $t = 100$s.

For the polychromatic sea state, only a single NWT length is tested, using the base mesh discretisation. Satisfying reflection coefficients, with maximum values of $< 7\%$, are observed.

*5) Absorption at FFB: Wave radiated from WEC:* For the considered free decay test case, an spherically shaped WEC, located in the centre of a NWT with length 12m, is given an initial amount of velocity and $t$ is limited to 100s. For comparison, a *no reflection* case is performed, which eliminates any reflection effects in the results, by increasing the NWT length such that any waves radiated from the WEC can not travel the distance to the FFB and back during the simulation time. Fig 17-(a) shows the free decay time series of the WEC velocity, measured in the test case NWT compared against a *no reflection* case. The velocity of the WEC is seen to exponentially decay to zero for both cases, however after approximately 20s the WEC velocity in the test case increases then decays again, and then again at approximately 40s. Fig 17-(b) shows the power spectrum of the time series data, from which it can be measured that the test case signal contains 1.29 times more energy (area under the curve) than the *no reflection* case. The test case spectrum contains spikes approximately every 0.05 Hz, corresponding to the 20s reflection period seen in the time series data. The 20s reflection period equates to the time taken for waves, with a group velocity determined for the peak period radiated by the WEC (1.4Hz, see 17-(b) ), to travel from the WEC to the NWM and then back to the WEC ($12m$). Results are summarised in Tab. III.

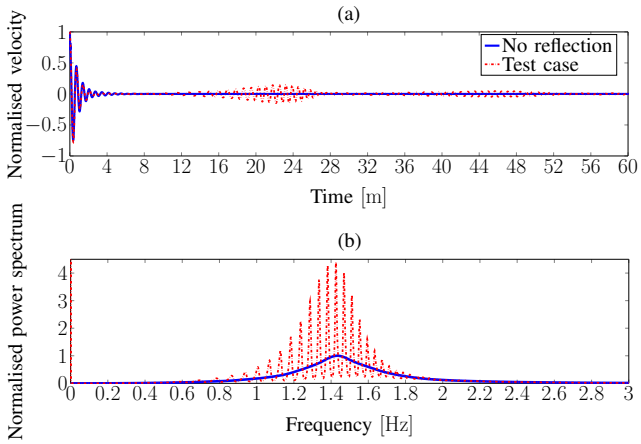


Fig. 17. (a) Time series of the WEC velocity in free decay experiment (b) The power spectrum of the time series

TABLE III
RESULTS FOR BENCHMARK CASES TO EVALUATE WAVE ABSORPTION

| Case | Quantification | *OLAFOAM* |
|---|---|---|
| 1) | Max. $A_{\text{standing wave}}/A_{\text{incident}}$ | 2.772 |
| | Node Location | $1/4\lambda$, $3/4\lambda$, ... |
| | Velocity Profile | pure z- and x-velocity at nodes resp. anti-nodes |
| 2) | Reflection Coefficient | 0.27 |
| | Fluid Mass Conservation | yes |
| 3) | Reflection Coefficient | $4 \cdot 10^{-3}$ |
| 4) | Reflection Coefficient | $< 0.07$ |
| 5) | Normalised spectral energy | 1.29 |

## VI. CONCLUSION

In this paper, a number of crucial NWM capabilities, for CFD-based NWTs, are defined, and a set of test cases, along with assessment criteria, for evaluation of NWMs are propsed. These tests aim to offer guidance in the NWM selection for a given problem. From the results presented in Sec. V the following conclusions are drawn:

- The quality and efficiency of numerical wave generation and absorption is highly dependent on the solver settings and the considered sea state
- An assessment of the quality and accuracy is thus necessary to prevent biased results

- The sample NWM, *OLAFOAM*, accurately generates the tested monochromatic deep water and the polychromatic sea state. However, for the considered shallow water wave conditions, considerable inaccuracies were observed
- The sample NWM is able to efficiently absorb waves for the tested shallow water and polychromatic sea state. Considerable reflections can be observed for the deep water case. Additionally, inaccuracies are observed for wave absorption at the generation boundary for the case tested
- Ultimately, quality and acceptable inaccuracy has to be judged and defined by user

## VII. Future Work

- In-detail investigation of the influence of mesh quality (i.e. aspect ratio and transition regions between different discretisation zones) on the NWM performance
- In-detail investigation of the representation of a given spectral distribution in order to determine the source of error for the shift in peak frequency observed in V-B3
- In-detail evaluation of time-series reproduction possibly including experimental data sets for quantitative assessment of this NWM capability
- Application of the proposed test cases on different available NWMs for a comparative study

## Acknowledgment

This paper is based upon work supported by Science Foundation Ireland under Grant No. 13/IA/1886.

## References

[1] P. Schmitt, H. Asmuth, and B. Elsaesser, "Optimising power take-off of an oscillating wave surge converter using high fidelity numerical simulations," *International Journal of Marine Energy*, vol. 16, pp. 196 – 208, 2016.

[2] E. B. Agamloh, A. K. Wallace, and A. von Jouanne, "Application of fluid-structure interaction simulation of an ocean wave energy extraction device," *Renewable Energy*, vol. 33, pp. 748–757, 2008.

[3] Y. Wei, T. Abadie, A. Henry, and F. Dias, "Wave ineraction with an Oscillating Wave Surge Converter. Part II: Slamming," *Ocean Engineering*, vol. 113, pp. 319 – 334, 2016.

[4] M. A. Bhinder, A. Babarit, L. Gentaz, and P. Ferrant, "Assessment of Viscous Damping via 3D-CFD Modelling of a Floating Wave Energy Device," in *Proceedings of the 9th European Wave and Tidal Energy Conference*, 2011.

[5] J. Davidson, C. Windt, G. Giorgi, R. Genest, and J. Ringwood, *11th OpenFOAM Workshop*. Springer, 2017, ch. Evaluationg of energy maximising control systems for wave energy converters using OpenFOAM.

[6] J. Spinneken and C. Swan, "Wave Generation and Absorption Using Force-controlled Wave Machines," in *Proceedings of the Nineteenth (2009) International Offshore and Polar Engineering Conference*, 2009.

[7] A. E. Maguire, "Hydrodynamics, control and numerical modelling of absorbing wavemakers," Ph.D. dissertation, The Univeristy of Edinburgh, 2011.

[8] P. Schmitt and B. Elsaesser, "A Review of Wave Makers for 3D numerical Simulations," in *Preceedings of the 6th International Conference on Computational Methods in Marine Engineering*, 2015.

[9] P. Lin and P. L.-F. Liu, "Internal wave-maker for navier-stokes equations models," *Journal of Waterway, Port, Coastal, and Ocean Engineering*, vol. 125, no. 4, pp. 207 – 215, 1999.

[10] J. Choi and S. B. Yoon, "Numerical simulations using momentum source wave-maker applied to RANS equation model," *Coastal Engineering*, vol. 56, no. 10, pp. 1043–1060, oct 2009.

[11] P. Higuera, J. L. Lara, and I. J. Losada, "Realistic wave generation and active wave absorption for NavierStokes models Application to OpenFOAM," *Coastal Engineering*, 2013.

[12] N. Jacobsen, D. R. Fuhrmann, and J. Fredsoe, "A wave generation toolbox for the open-source CFD library: OpenFoam(R)," *International Journal for Numerical Methods in Fluids*, 2012.

[13] L. Chen, "Modelling of marine renewable energy," Ph.D. dissertation, Univeristy of Bath, Department of Architecture and Civil Engineering, 2015.

[14] S. Saincher and J. Banerjee, "On wave damping occurring during source-based generation of steep waves in deep and near-shallow water," *Ocean Engineering*, vol. 135, pp. 98–116, may 2017.

[15] H. K. Versteeg, *An Introduction to Computational Fluid Dynamics*, W. Malalasekera, Ed. Pearson Education Limited, 2007.

[16] C. W. Hirt and B. D. Nichols, "Volume of Fluid (VOF) Method for the Dynamics of Free Boundaries," *Journal of Computational Physics*, 1981.

[17] E. Berberovic, N. van Hinsberg, S. Jakirlic, I. Roisman, and C. Tropea, "Drop impact onto a liquid layer of finite thickness: Dynamics of the cavity evolution," *Physical Review E - Statistical, Nonlinear, and Soft Matter Physics*, 2009.

[18] P. Schmitt, "Investigation of the near flow field of bottom hinged flap type wave energy converters," Ph.D. dissertation, School of Planning, Architecture and Civil Engineering, Queen's Univeristy Belfast, 2013.

[19] A. Clement, "Coupling of Two Absorbing Boundary Conditions for 2D Time-Domain Simulations of Free Surface Gravity Waves," *Jounral of Computational Physics*, vol. 126, pp. 139 – 151, 1996.

[20] M. Anbarsooz, M. Passandideh-Fard, and M. Moghiman, "Numerical simulation of a submerged cylindrical wave energy converter," *Renewable Energy*, vol. 64, pp. 132–143, apr 2014.

[21] P. Higuera, "Application of computational fluid dynamics to wave action on structures," Ph.D. dissertation, University of Cantabria, School of Civil Engineering, 2015.

[22] H. A. Schaeffer and G. Klopman, "Review of multidirectional active wave absorption methods," *Journal of Waterway, Port, Coastal and Ocean Engineering*, 2000.

[23] R. Peric and M. Abdel-Maksoud, "Generation of free-surface waves by localized source terms in the continuity equation," *Ocean Engineering*, vol. 109, pp. 567–579, nov 2015.

[24] G. B. Airy, "Tides and waves," 1841.

[25] I. A. Svendsen, *Introduction to Nearshore Hydrodynamics*. World Scientific Pub Co. Inc., 2005.

[26] S. Michele, P. Sammarco, and M. d'Errico, "The optimal design of a flap gate array in front of a straight vertical wall: Resonance of the natural modes and enhancement of the exciting torque," *Ocean Engineering*, vol. 118, pp. 152–164, may 2016.

[27] D. Sarkar, E. Renzi, and F. Dias, "Effect of a straight coast on the hydrodynamics and performance of the oscillating wave surge converter," *Ocean Engineering*, vol. 105, pp. 25–32, sep 2015.

[28] D. Evans, "The maximum efficiency of wave-energy devices near coast lines," *Applied Ocean Research*, vol. 10, no. 3, pp. 162–164, jul 1988.

[29] E. Mansard and E. Funke, "The measurement of incident and reflected spectra using a least squares method," in *Coastal Engineering 1980*. American Society of Civil Engineers (ASCE), mar 1980.

[30] H. G. Weller, G. Tabor, H. Jasak, and C. Fureby, "A tensorial approach to computational continuum mechanics using object-oriented techniques," *Computers in Physic*, vol. 12, no. 6, pp. 620 – 631, 1998.

[31] T. T. Loh, D. Greaves, T. Maeki, M. Vuorinen, D. Simmonds, and A. Kyte, "Numerical modelling of the WaveRoller device using OpenFOAM," in *Proceedings of the 3rd Asian Wave & Tidal Energy Conference*, 2016.

[32] J. Davidson, M. Cathelain, L. Guillemet, T. Le Huec, and J. Ringwood, "Implementation of an openfoam numerical wave tank for wave energy experiments," in *Proceedings of the 11th European Wave and Tidal Energy Conference*, 2015.

[33] IH Cantarbia. (2017) IHFOAM website. Last accessed 2017-07-08. [Online]. Available: http://ihfoam.ihcantabria.com/

[34] P. B. Garcia-Rosa, R. Costello, F. Dias, and J. V. Ringwood, "Hydrodynamic modelling competition - overview and approach," in *Proceedings of the ASME 2015 34th International Conference on Ocean, Offshore and Arctic Engineering*, 2015.

[35] O. Faltinsen, *Sea Loads on Ships and Offshore Structures*. Cambridge University Press, 1998.